

ZAMM · Z. angew. Math. Mech. **78** (1998) 0, 1–22

BUTZ, T.; VON STRYK, O.

## Modelling and Simulation of Electro- and Magnetorheological Fluid Dampers

*Electro- and magnetorheological fluids are smart, synthetic fluids changing their viscosity from liquid to semi-solid state within milliseconds if a sufficiently strong electric or magnetic field is applied. When used in suitable devices, they offer the innovative potential of very fast, adaptively controllable interfaces between mechanical devices and electronic control units. This paper gives an overview on the basic properties of electro- and magnetorheological fluids and discusses various phenomenological models for whole devices and their applications. Numerical simulation results are presented for the passive suspension of a quarter vehicle model.*

Keywords: electro- and magnetorheological fluid devices, phenomenological models, numerical simulation, passive suspension

MSC (1991): 65C20, 76A05

### 1 Introduction

Electro- (ER) and magnetorheological (MR) fluids are colloidal suspensions which exhibit large reversible changes in flow properties such as the apparent viscosity when subjected to sufficiently strong electric and magnetic fields respectively (WINSLOW [51]). They usually consist of micron-sized polarisable or magnetisable solid particles dissolved in a non-conducting liquid like mineral or silicone oil. In general, the composition of ER and MR fluids exhibits a broad diversity concerning solvent, solute and additives (see for example BLOCK and KELLY [5], CARLSON and SPENCER [12]).

In recent years, ER and MR fluids have attracted considerable interest due to their wide range of use in vibration dampers for vehicle suspension systems, machinery mounts or even seismic protection of structures; their stiffness and damping capabilities can be adjusted very quickly by applying a suitable electric or magnetic field (STANWAY et al. [46]).

ER and MR fluid dampers enable active and semi-active vibration control systems with reaction times in the range of milliseconds and, additionally, low power requirements when using MR fluids. Due to their rather simple mechanical design which involves only few moving parts they ensure high technical reliability and exhibit almost no wear. Thus, continuously adjustable ER and MR fluid devices offer the **innovative potential** of robust and fast controllable interfaces between mechanical components and electronic control units.

Scientific challenges in the field of electro- and magnetorheological fluids and devices consist in:

1. **The development of (optimal) control strategies** for ER and MR fluid devices: *Because of the intrinsically nonlinear nature of semi-active control devices, development of output feedback control strategies that are practically implementable and can fully utilize the capabilities of these unique devices is another important, yet challenging, task* (SPENCER [43]).

Though, to develop suitable control algorithms for electro- and magnetorheological fluid devices mathematical and physical models are needed that can accurately reproduce their nonlinear behaviour.

2. **The mathematical modelling and numerical simulation** of ER and MR fluids and devices: *Note: The mechanism of ER fluids is not well understood and hence what is theoretically possible is not known* (HARTSOCK et al. [22], p. 1310).

The outline of this paper is as follows: After a description of ER and MR mechanisms and fluid properties several phenomenological models for ER and MR fluid devices are presented according to results of the current research. Their validity is discussed as far as comparisons with experimental data have been reported within the literature. Finally, different discrete element models are applied to a MR fluid vibration damper, and its operation is simulated numerically.

## 2 Electro- and magnetorheological mechanisms and fluid properties

It is commonly agreed that the main mechanism of the ER response is based on some form of polarisation due to the dielectric mismatch between the suspended particles and the solvent (POWELL [42], BONNECAZE and BRADY [6]). A qualitative explanation accounts for the particles as dipoles. Accordingly, the electrostatic forces cause the formation of particle chains in the direction of the electric field. The tendency of columnar formation has been observed experimentally as well as the development of larger particle clusters with increasing particle concentration (GAST and ZUKOSKI [18], KLINGENBERG et al. [31]). However, POWELL [42] mentions another proposed mechanism of the induced polarisation of an ionic double layer.

Electrorheological fluids exhibit a yield phenomenon when subjected to a sufficiently large electric field. A yield stress increasing with the field strength must be overcome to start fluid flow (between stationary electrodes) or shearing of the fluid (between moving electrodes) perpendicular to the applied field (Figure 1). The exponents of the power law  $\tau_y = E^n$  relating the field strength  $E$  to the yield stress  $\tau_y$  are reported to range from 1.2 to 2.5 depending on the consistency of the suspension (GAVIN et al. [19]). In terms of the above described mechanisms the yield point may be related to the breakage of particle chains. In the pre-yield region ER fluids behave like elastic solids, resulting from chain stretching with some occasional rupture; the post-yield region reflects an equilibrium between chain rupture and reformation, the fluid exhibits viscous properties (CHOI et al. [13], GAMOTA and FILSKO [17]). The structural processes, more precisely described by POWELL [42] and KAMATH et al. [26], differ according to the respective operating modes (cf. Section 3, Figure 1), but obviously they are of minor significance for modelling ER and MR fluid devices in general.

BONNECAZE and BRADY [6] proposed a molecular-dynamics-like simulation of an ER suspension subjected to both shear flow and an orthogonal electric field. The method allows for hydrodynamic, e. g., viscous, inter-particle interactions determined by Stokesian dynamics as well as for electrostatic forces that are derived from the system's electrostatic energy. The simulation is able to predict the apparent viscosity in accordance with the experimental data. Combined with an idealised chain model for the microstructure of the activated fluid it can further approximate the experimentally observed values for the yield stress (BONNECAZE and BRADY [7]). Except for small shear rates (expressed in terms of the so-called Mason number) the results of the simulation match with the Bingham plastic model described in the next section (BONNECAZE and BRADY [6]). Recently, ENGELMANN et al. [16] proposed an extension of the classical Bingham model which goes beyond pure shear flows and enables the simulation of electrorheological fluids in complex geometries [23].

In the case of magnetorheological fluids a magnetic field causes the chain-like arrangement of the suspended particles by inducing a magnetic moment. In addition, MR fluids exhibit a yield stress increasing with the applied field, and both a pre-yield region, characterised by elastic properties, and a post-yield region, characterised by viscous properties (JOLLY et al. [25]). Due to their qualitatively similar behaviour phenomenological models of ER and MR fluid devices can mostly be applied to either material (KAMATH and WERELEY [27]).

<i>Property</i>	<i>ER Fluid</i>	<i>MR Fluid</i>
<i>response time</i>	milliseconds	milliseconds
<i>plastic viscosity <math>\eta</math> (at 25° C)</i>	0.2 to 0.3 Pa·s	0.2 to 0.3 Pa·s
<i>operable temperature range</i>	+10 to +90° C (ionic, DC) -25 to +125° C (non-ionic, AC)	-40 to 150° C
<i>power supply (typical)</i>	2 to 5 kV 1 to 10 mA (2 to 50 watts)	2 to 25 V 1 to 2 A (2 to 50 watts)
<i>maximum yield stress <math>\tau_y</math></i>	2 to 5 kPa (at 3 to 5kV/mm)	50 to 100 kPa (at 150 to 250 kA/m)
<i>maximum field</i>	ca. 4 kV/mm	ca. 250 kA/m
$\eta/\tau_y^2$	$10^{-7}$ to $10^{-8}$ s/Pa	$10^{-10}$ to $10^{-11}$ s/Pa
<i>density</i>	1 to 2 g/cm <sup>3</sup>	3 to 4 g/cm <sup>3</sup>

Table 1: Typical properties of some electro- and magnetorheological fluids, cf. CARLSON and SPENCER [12], LAMPE [33], LORD CORPORATION [36], WEISS et al. [48].

Some properties of typical electro- and magnetorheological fluids are provided in Table 1. Exhibiting about the same response time and plastic viscosity  $\eta$  as their ER analogues, MR fluids are less sensitive to impurities, such as water, usually occurring during manufacturing and usage. They have a larger operating temperature range, and they can be controlled with a considerably lower voltage (SPENCER et al. [44]). Moreover, the yield stress achievable with MR suspensions is at least an order of magnitude greater just as the material property  $\eta/\tau_y^2$ , so

that MR devices only require a comparatively small amount of fluid and space (WEISS et al. [48], SPENCER [43]). However, since often iron is used as a solute, the density of MR fluids is significantly higher than for typical ER suspensions. In addition, a greater variety of materials is available for ER fluids, and electric fields are often more suitable for complex geometries and small dimensions (BÖSE [8]).

### 3 Phenomenological models for ER and MR fluid devices

To take maximum advantage of electro- and magnetorheological fluids in control applications a reliable method is needed to predict their nonlinear response. Several phenomenological models characterising the behaviour of ER and MR fluid devices have been presented. These models concern ER test devices (GAMOTA and FILISKO [17], EHRGOTT and MASRI [15], POWELL [42], GAVIN et al. [19], [20], KAMATH and WERELEY [28]) as well as ER and MR dampers for both seismic protection (MAKRIS et al. [37], [38], BURTON et al. [11], SPENCER et al. [44], DYKE et al. [14]) and vehicle applications (STANWAY et al. [45], KAMATH et al. [26], KAMATH and WERELEY [27], [29]). But despite the promise of controllable fluids most of the current models solely reproduce the ER and MR behaviour for constant field strengths. So far few concepts have been developed that allow for varying field strengths as needed for the design of active control strategies.

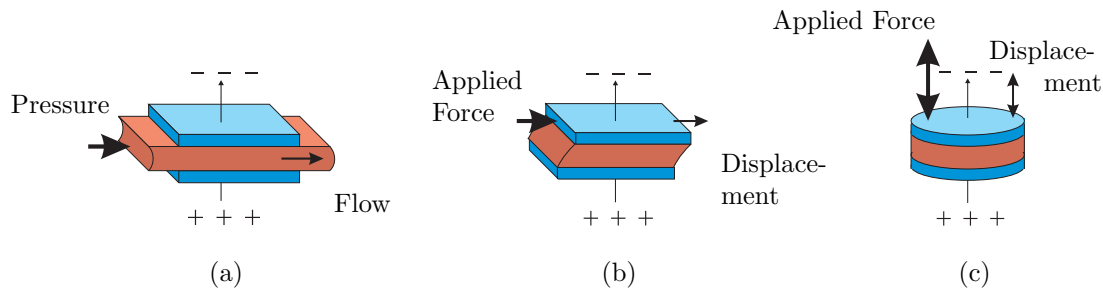


Figure 1: Basic operating modes of electro- and magnetorheological fluid devices. (a) Valve mode. (b) Direct shear mode. (c) Squeeze-flow mode.

Most often, the considered devices operate in the valve (flow) mode, the direct shear mode or a combination of the two modes (STANWAY et al. [46]). In a control valve the electro-rheological fluid is constrained between stationary electrodes, and its resistance to flow is accommodated by adjusting the applied field (Figure 1a); frequently the performance of hydraulic piston/cylinder dampers is controlled in this way. In the latter mode, the fluid is subjected to direct shear between electrodes translating or rotating perpendicular to the field (Figure 1b). Few attention is paid to rheological devices employing the most recently introduced mode of squeeze-flow. This operating mode involves electrode motion in the direction of the applied field (Figure 1c); therefore the field strength continually varies according to the electrode distance (STANWAY et al. [46]). In case of magnetorheological fluids the magnetic poles take the place of the electrodes.

The proposed models do not strictly distinguish between the different modes of operation; but commonly adjustments have to be made corresponding to the design and the components of the respective devices. For reasons of wider commercial availability the recent research has mainly concentrated on modelling the ER fluid response (KAMATH and WERELEY [29]). But due to their similar behaviour little difference is made between electro- and magnetorheological materials in the following survey. It is useful to distinguish between models which qualitatively simulate the ER or MR response and are fitted to experimental results by adjusting few parameters (parametric models) and models which are entirely based on the performance of a specific fluid device (non-parametric models).

#### 3.1 Parametric models

Parametric models are represented by a mathematical function whose coefficients are determined rheologically, i. e., the parameter values are adjusted until the quantitative results of the model closely match the experimental data. Thus, the dynamic response of ER and MR fluid devices is reproduced by a semi-empirical relationship. Numerous parametric models can easily be described by an arrangement of mechanical elements such as springs and viscous dashpots.

### 3.1.1 Bingham model

Most commonly the behaviour of ER and MR fluids is described by the Bingham plastic model. An ideal Bingham body behaves as a solid until a minimum yield stress  $\tau_y$  is exceeded and then exhibits a linear relation between the stress and the rate of shear or deformation. Accordingly the shear stress  $\tau$  developed in the fluid is given by

$$\tau = \tau_y \cdot \text{sgn}(\dot{\gamma}) + \eta \dot{\gamma} \quad (1)$$

where  $\dot{\gamma}$  is the (shear) strain rate and  $\eta$  denotes the plastic viscosity of the fluid, i. e., the (Newtonian) viscosity at zero field (GAVIN et al. [19]).

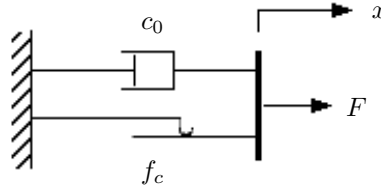


Figure 2: Bingham model (SPENCER et al. [44]).

In order to characterise the ER damping mechanism STANWAY et al. [45] proposed a mechanical model, commonly referred to as the Bingham model, that combines viscous and Coulomb friction. The mechanical analogue, a Coulomb friction element in parallel with a viscous dashpot, is shown in Figure 2. In this model, the force  $F$  generated by the ER or MR fluid device is given by

$$F = f_c \cdot \text{sgn}(\dot{x}) + c_0 \dot{x} \quad (2)$$

where  $\dot{x}$  denotes the velocity attributed to the external excitation, and where the damping coefficient  $c_0$  and the frictional force  $f_c$  are related to the fluid's viscosity and the field dependent yield stress respectively (SPENCER et al. [44]).

The Bingham model accounts for electro- and magnetorheological fluid behaviour beyond the yield point, i. e., for fully developed fluid flow or sufficiently high shear rates. However, it assumes that the fluid remains rigid in the pre-yield region. Thus, the Bingham model does not describe the fluid's elastic properties at small deformations and low shear rates which is necessary for dynamic applications (KAMATH and WERELEY [28]). A comparison between the predicted force-velocity characteristic and the result of experiments conducted by SPENCER et al. [44] is provided in Figure 3.

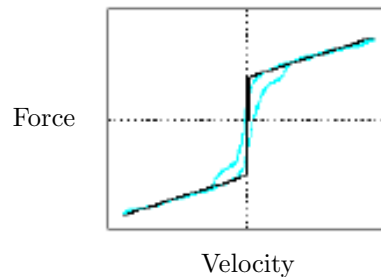


Figure 3: Comparison between the predicted ( — ) and the experimentally obtained ( — ) force-velocity characteristic for the Bingham model (SPENCER et al. [44]).

### 3.1.2 Extended Bingham model

GAMOTA and FILISKO [17] presented an extension of the Bingham model to describe the ER fluid behaviour in the pre-yield and the post-yield region as well as at the yield point. This viscoelastic-plastic model consists of the Bingham model in series with the three-parameter element of a linear solid (Zener element) as shown in Figure 4. The force in this system is given by

$$F = \begin{cases} \begin{matrix} c_0 \dot{x}_1 + f_c \cdot \text{sgn}(\dot{x}_1) \\ k_1(x_2 - x_1) + c_1(\dot{x}_2 - \dot{x}_1) \\ k_2(x_3 - x_2) \end{matrix} & , \quad |F| > f_c \\ \begin{matrix} k_1(x_2 - x_1) + c_1 \dot{x}_2 \\ k_2(x_3 - x_2) \end{matrix} & , \quad |F| \leq f_c \end{cases} \quad (3)$$

where again the damping coefficient  $c_0$  and the frictional force  $f_c$  in the Bingham model account for the plastic viscosity and the yield stress respectively. The field dependent parameters  $c_1$ ,  $k_1$  and  $k_2$  are associated with the fluid's elastic properties in the pre-yield region (GAMOTA and FILISKO [17], SPENCER et al. [44]).

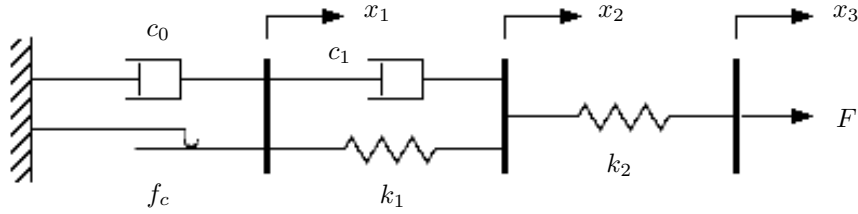


Figure 4: Extended Bingham model (SPENCER et al. [44]).

As depicted in Figure 5, the extended Bingham model qualitatively describes the hysteretic response of the MR fluid device considered by SPENCER et al. [44]. However, the resulting system of ordinary differential equations is extremely stiff due to the nonlinear Coulomb friction element. Thus, the numerical simulation with explicit integration methods requires very small time steps (cf. STOER and BULIRSCH [47]).

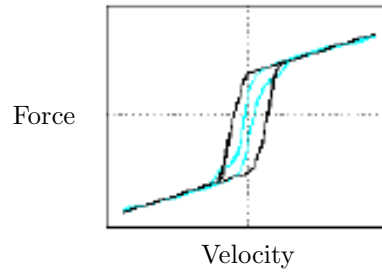


Figure 5: Comparison between the predicted ( — ) and the experimentally obtained ( — ) force-velocity characteristic for the extended Bingham model (SPENCER et al. [44]).

### 3.1.3 Three element model

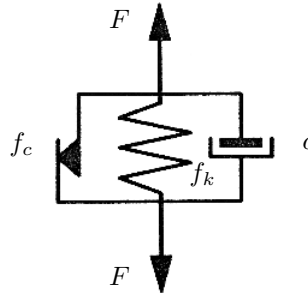


Figure 6: Three element model (POWELL [42]).

Focussing on predicting the behaviour of an ER fluid device POWELL [42] proposed a mechanical analogue consisting of a viscous damper, a nonlinear spring and a frictional element in parallel (Figure 6). In order to reproduce the hysteretic force-velocity characteristic that is observed experimentally (cf. Figure 7b), the Coulomb friction force  $f_c$  is modelled with static and dynamic friction coefficients  $f_{cs}$  and  $f_{cd}$  respectively. Furthermore, to facilitate the numerical integration smoothing functions are introduced for the friction force instead of the signum function. Hence,

$$f_c = \begin{cases} f_{cs} \left( 1 + (f_{cd}/f_{cs}) \cdot \exp(-a|\dot{z}|) \right) \cdot \tanh(e\dot{z}) & , \dot{z} \cdot \ddot{z} \geq 0 \\ f_{cd} \left( 1 - \exp(-b|\dot{z}|) \right) \cdot \tanh(e\dot{z}) & , \dot{z} \cdot \ddot{z} < 0 \end{cases} \quad (4)$$

where  $z$  is the displacement transmitted to the ER fluid device, and  $\dot{z}$  and  $\ddot{z}$  denote the corresponding velocity and acceleration respectively. The force generated by the device is given by

$$F = f_c + f_k + c\dot{z} \quad (5)$$

where  $f_k = k \cdot \tanh(dz)$  is the nonlinear force of a softening spring. In this model, the field-dependent values of the damping parameters  $f_{cs}$ ,  $f_{cd}$ ,  $a$ ,  $b$ ,  $c$  and  $e$  as well as the elastic parameters  $d$  and  $k$  are fitted to the experimental results. A comparison between the predicted and the observed behaviour of the ER device is provided in Figure 7.

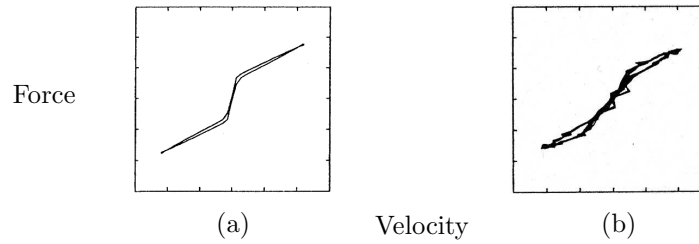


Figure 7: Comparison between the predicted (a) and the experimentally obtained (b) force-velocity characteristic for the three element model (POWELL [42]).

The three element model predicts the experimental ER response well, and it is numerically easier to deal with than the extended Bingham model. However, it cannot always represent the experimentally observed variations in the forces (POWELL [42]), and it demands a large number of parameter values depending on the applied field strength and the specific external excitation, as it is suggested by the presented simulation data.

### 3.1.4 BingMax model

A discrete element model with similar components, referred to as the BingMax model, is reviewed by MAKRIS et al. [38]. It consists of a Maxwell element in parallel with a Coulomb friction element as depicted in Figure 8.

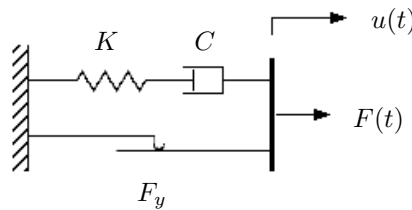


Figure 8: BingMax model (MAKRIS et al. [38]).

The force  $F(t)$  in this system is given by

$$F(t) = K \int_0^t \exp\left(-\frac{t-\tau}{\lambda}\right) \dot{u}(\tau) d\tau + F_y \cdot \operatorname{sgn}[\dot{u}(t)] \quad (6)$$

where  $\lambda = C/K$  is the quotient of the damping constant  $C$  and the spring stiffness  $K$ , and  $F_y$  denotes the permanent friction force. Equivalently the constituting Equation (6) can be written as

$$F(t) + \lambda \cdot \frac{dF(t)}{dt} = C \cdot \dot{u}(t) + F_y \cdot \operatorname{sgn}[\dot{u}(t)] \quad (7)$$

(see for example BIRD et al. [4]).

To evaluate the performance of the BingMax model the predicted behaviour of the electrorheological device was compared with its experimental response to an earthquake excitation. The model is analysed in more detail by BURTON [10].

### 3.1.5 Bouc-Wen model

In their survey of phenomenological models SPENCER et al. [44] presented the so-called Bouc-Wen model in order to characterise the behaviour of a MR fluid damper. The concept is based on an approach due to WEN [49]. It is supposed to reproduce the response of hysteretic systems to random excitations [9].

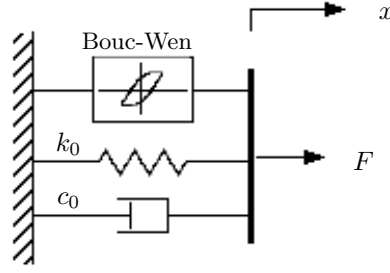


Figure 9: Bouc-Wen model (SPENCER et al. [44]).

A mechanical analogue of the Bouc-Wen model is shown in Figure 9. The force generated by the device is given by

$$F = c_0 \dot{x} + k_0(x - x_0) + \alpha z \quad (8)$$

where the hysteretic component  $z$  satisfies

$$\dot{z} = -\gamma |\dot{x}| z |z|^{n-1} - \beta \dot{x} |z|^n + \delta \dot{x}. \quad (9)$$

By adjusting the parameter values  $\alpha$ ,  $\beta$ ,  $\gamma$ ,  $\delta$  and  $n$  it is possible to control the shape of the force-velocity characteristic; an initial displacement  $x_0$  of the spring was incorporated into the model to allow for the presence of an accumulator in the considered damper.

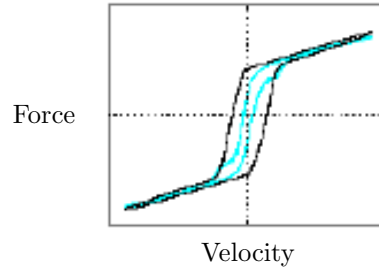


Figure 10: Comparison between the predicted (—) and the experimentally obtained (—) force-velocity characteristic for the Bouc-Wen model (SPENCER et al. [44]).

The Bouc-Wen model is well suited for the numerical simulation, since the resulting dynamic equations are less stiff than for the extended Bingham model. But as it is depicted in Figure 10, it cannot reproduce the experimentally observed roll-off in the yield region, i. e., for velocities with a small absolute value and an operational sign opposite to the sign of the acceleration.

### 3.1.6 Modified Bouc-Wen model

To better predict the response of the MR damper in the region of the yield point SPENCER et al. [44] proposed an extension of the Bouc-Wen model which is depicted in Figure 11. The equations for the force in this system are given by

$$\begin{aligned} F &= \alpha z + c_0(\dot{x} - \dot{y}) + k_0(x - y) + k_1(x - x_0) \\ &= c_1 \dot{y} + k_1(x - x_0) \end{aligned} \quad (10)$$

where

$$\dot{z} = -\gamma |\dot{x} - \dot{y}| z |z|^{n-1} - \beta(\dot{x} - \dot{y}) |z|^n + \delta(\dot{x} - \dot{y}) \quad (11)$$

and

$$\dot{y} = \frac{1}{c_0 + c_1} [\alpha z + c_0 \dot{x} + k_0(x - y)]. \quad (12)$$

The hysteretic component  $z$  accounts for the time history of the response (DYKE et al. [14]). The spring  $k_1$  and its initial displacement  $x_0$  allow for both the additional stiffness and the force offset produced by the presence of an accumulator. The latter was included into the considered damper for reasons of pressure compensation.

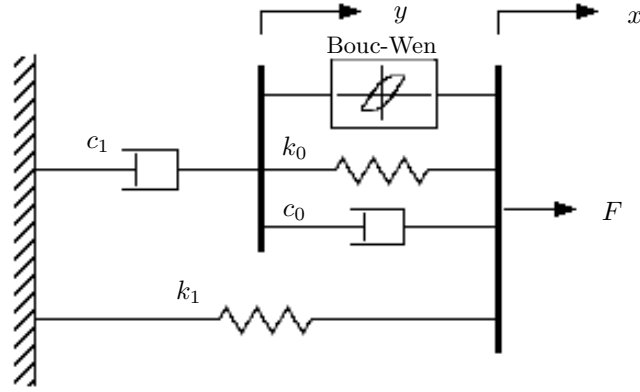


Figure 11: Modified Bouc-Wen model (SPENCER et al. [44]).

To obtain a model which is valid for varying magnetic field strengths the parameters are assumed to depend linearly on the voltage  $v$  applied to the current driver, i. e.,

$$\alpha = \alpha(u) = \alpha_a + \alpha_b u \quad (13)$$

$$c_1 = c_1(u) = c_{1a} + c_{1b} u \quad (14)$$

$$c_0 = c_0(u) = c_{0a} + c_{0b} u \quad (15)$$

where  $u$  is governed by

$$\dot{u} = -\eta(u - v). \quad (16)$$

The first order filter given by Equation (16) was introduced to allow for the fluid's dynamics of reaching rheological equilibrium.

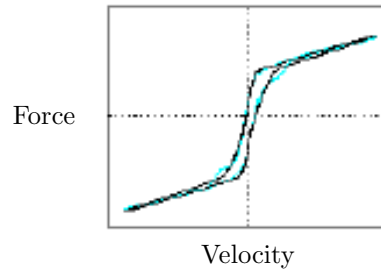


Figure 12: Comparison between the predicted (—) and the experimentally obtained (—) force-velocity characteristic for the modified Bouc-Wen model (SPENCER et al. [44]).

A comparison between the force-velocity characteristic predicted by the modified Bouc-Wen model and the result of experiments conducted by SPENCER et al. [44] is provided in Figure 12. The model is able to accurately reproduce the MR fluid behaviour, even over a broad range of operating conditions (SPENCER et al. [44]). Moreover, its parameter values are independent of the applied voltage and need not be estimated anew for different field strengths. However, the proposed model is highly dependent on the design and the components of the specific magnetorheological fluid device. In particular, an additional spring was incorporated to account for the accumulator present in the considered damper.

### 3.1.7 Nonlinear viscoelastic-plastic model

The viscoelastic-plastic model presented by KAMATH and WERELEY [28] combines two linear shear flow mechanisms with nonlinear weighting functions in order to characterise the response of an ER fluid device.

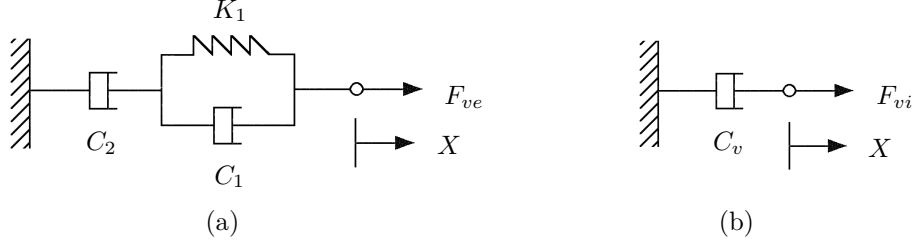


Figure 13: Viscoelastic-plastic model (KAMATH and WERELEY [28]).  
 (a) Viscoelastic mechanism. (b) Viscous mechanism.

In the pre-yield region the fluid's behaviour is simulated by the three-parameter element of a linear fluid (Jeffreys model) as depicted in Figure 13a. The viscoelastic force  $F_{ve}$  generated by this system is governed by

$$F_{ve} + \frac{C_1 + C_2}{K_1} \cdot \frac{dF_{ve}}{dt} = C_2 \dot{X} + \frac{C_1 C_2}{K_1} \cdot \ddot{X} \quad (17)$$

where  $C_1$ ,  $C_2$  and  $K_1$  denote the parametric damping and stiffness constants respectively, and where  $X$  is the displacement transmitted to the device. In the post-yield region the ER response is represented by the viscous relationship

$$F_{vi} = C_v \dot{X} \quad (18)$$

where the damping coefficient  $C_v$  is related to the apparent viscosity of the fluid (Figure 13b).

The transition from the pre-yield to the post-yield regime is performed by nonlinearly combining the viscoelastic and viscous components  $F_{ve}$  and  $F_{vi}$  to the net force

$$F = F_{ve} S_{ve} + F_{vi} S_{vi}. \quad (19)$$

The shape functions

$$S_{ve} = \frac{1}{2} \left[ 1 - \tanh\left(\frac{\alpha - \alpha_y}{4\varepsilon_y}\right) \right] \quad (20)$$

and

$$S_{vi} = \frac{1}{2} \left[ 1 + \tanh\left(\frac{\alpha - \alpha_y}{4\varepsilon_y}\right) \right] \quad (21)$$

depend on the velocity  $\alpha$  non-dimensionalised with respect to its amplitude, the yield parameter  $\alpha_y$  which is correlated with the fluid's yield point and a smoothing parameter  $\varepsilon_y$  (KAMATH and WERELEY [29]). A scheme of the force-displacement relationship is shown in Figure 14;  $L_{ve}$  and  $L_{vi}$  are the linear operators representing the Equations (17) and (18) respectively.

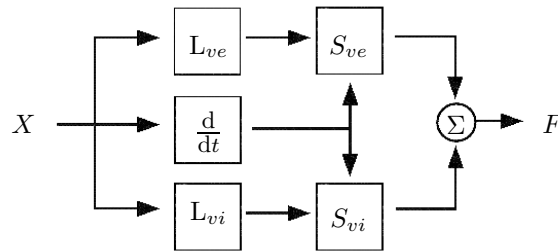


Figure 14: Scheme of the viscoelastic-plastic model (KAMATH and WERELEY [28]).

The values for the parametric constants were found to be strong functions of the electric field, and it was proposed to approximate the coefficients associated with the viscoelastic and plastic properties as polynomial functions of the field strength. Comparisons between predicted and experimental data showed that the model is able to reproduce the nonlinear effects of the ER behaviour qualitatively. In addition, the model is numerically robust due to the linearity of the parallel shear flow mechanisms (KAMATH and WERELEY [28]).

### 3.1.8 Augmented nonlinear viscoelastic-plastic model

To further reproduce the force-velocity characteristic of the considered ER fluid device KAMATH and WERELEY [29] extended the nonlinear model described above. In the pre-yield region the friction force  $F_c$  weighted by a shape function  $S_c$  was added to allow for Coulomb-like sticktion effects observed at low velocities. Thus, the force  $F_{by}$  generated in the pre-yield branch is given by

$$F_{by} = F_{ve} + S_c F_c \quad (22)$$

where

$$S_c = \frac{1}{2} \tanh\left(\frac{\dot{X}}{4\varepsilon_c}\right), \quad (23)$$

and  $\varepsilon_c$  is a smoothing factor. The viscoelastic component  $F_{ve}$  is governed by Equation (17).

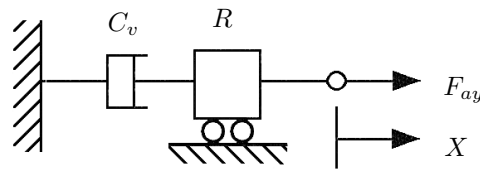


Figure 15: Inertial mechanism of the augmented viscoelastic-plastic model (KAMATH and WERELEY [29]).

To account for fluid inertia effects beyond the yield point KAMATH and WERELEY [29] introduced the viscous and inertial mechanism depicted in Figure 15. Thus, the force  $F_{ay}$  in the post-yield branch is given by

$$F_{ay} = C_v \dot{X} + R\ddot{X}. \quad (24)$$

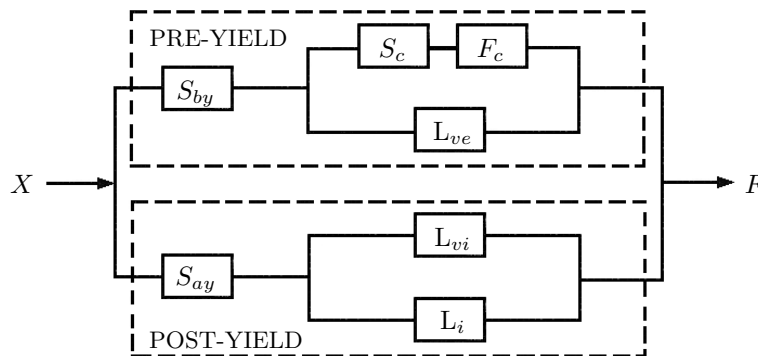


Figure 16: Scheme of the augmented viscoelastic-plastic model (KAMATH and WERELEY [29]).

Both shear flow mechanisms are combined by the two nonlinear weighting functions  $S_{by} = S_{ve}$  (Eq. 20) and  $S_{ay} = S_{vi}$  (Eq. 21) yielding the nonlinear network depicted in Figure 16. The total force  $F$  generated by this augmented viscoelastic-plastic model is given by

$$F = S_{by} F_{by} + S_{ay} F_{ay}. \quad (25)$$

A comparison between the force-velocity characteristic predicted by the proposed model and obtained from experimental results is provided in Figure 17. The model precisely depicts the behaviour of the considered ER fluid device at different field strengths and displacement amplitudes (KAMATH and WERELEY [29]). The added mechanisms, such as the friction component  $F_c$ , largely depend on the design of the considered damper, but they can be adjusted by choosing suitable parameter values. Moreover, the nonlinear combination of linear flow mechanisms is numerically tractable.

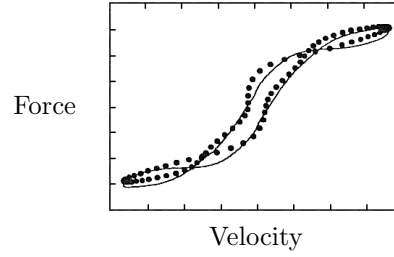


Figure 17: Comparison between the predicted (—) and the experimentally obtained (•••••) force-velocity characteristic for the augmented viscoelastic-plastic model (KAMATH and WERELEY [29]).

### 3.1.9 Other models

For the analysis of ER or MR fluid devices operating in the squeeze-flow mode the equation governing the shear stress  $\tau$  in the Bingham plastic model can be generalised to the bi-viscous relationship

$$\tau = \begin{cases} \eta_r \dot{\gamma} & , \quad |\tau| < \tau_1 \\ \tau_0 + \eta \dot{\gamma} & , \quad |\tau| > \tau_1 \end{cases} \quad (26)$$

where  $\dot{\gamma}$  is the strain rate, and  $\eta_r$  and  $\eta$  are related to the elastic and the viscous fluid properties respectively (STANWAY et al. [46]). The yield parameters  $\tau_0$  and  $\tau_1$  satisfy

$$\tau_0 = \tau_1 \left( 1 - \frac{\eta}{\eta_r} \right), \quad (27)$$

as it is illustrated in Figure 18. The Bingham plastic model is obtained for  $\eta_r \rightarrow \infty$ .

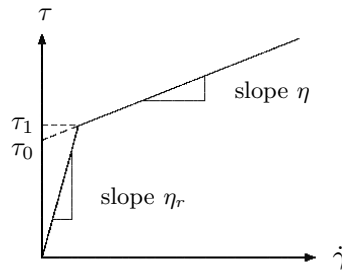


Figure 18: Bi-viscous model (STANWAY et al. [46]).

MAKRIS et al. [37] developed a continuum mechanics constitutive model to characterise the behaviour of an ER fluid prototype damper. The fluid's motion in the valve of the damper was approximated by Hagen-Poiseuille flow theory assuming laminar, one-dimensional flow through a stationary annular duct. The authors derived a linear first-order equation with variable coefficients to account for the elastic-viscoplastic properties of the fluid:

$$\frac{d\tau}{dt} + \frac{G\dot{\gamma}}{\eta_0\dot{\gamma} + \tau_y \text{sgn}(\dot{\gamma})} \cdot \tau = G\dot{\gamma} \quad (28)$$

where  $\eta_0$ ,  $\tau_y$  and  $G$  denote the plastic viscosity, the yield stress and the elastic shear modulus of the fluid respectively. However, the model considerably depends on the physical properties of the fluid and the design of the damper (MAKRIS et al. [38]).

## 3.2 Non-parametric models

Non-parametric models are entirely based on the performance of a specific ER or MR fluid device. Commonly an elevated amount of experimental data, obtained by observing the electro- or magnetorheological response to different excitations under varying operating conditions, is used to predict the device's response to random excitations.

### 3.2.1 Chebyshev polynomial fit

EHRGOTT and MASRI [15] used a Chebyshev polynomial fit to approximate the force generated by an ER test device. For fixed electric field strength (and fixed exciting frequency) the restoring force  $F$  of the ER fluid device was predicted by an analytical function  $\hat{F}$  constructed by two-dimensional orthogonal Chebyshev polynomials

$$F(x, \dot{x}) \approx \hat{F}(x, \dot{x}) = \sum_{i,j=0}^m C_{ij} T_i(x') T_j(\dot{x}') \quad (29)$$

where the  $C_{ij} \in \mathbb{R}$  denote the two-dimensional Chebyshev coefficients, and  $m$  is the maximum degree of the basis polynomials  $T_i$ . The values  $x'$  and  $\dot{x}'$  are obtained by normalising the displacement  $x$  and the velocity  $\dot{x}$  that are associated with the external excitation to the interval  $[-1, +1]$ . In the same way, the force  $F$  can be determined as a function of the velocity  $\dot{x}$  and the acceleration  $\ddot{x}$ .

GAVIN et al. [20] extended this curve-fitting method to three dimensions. They related the restoring force  $F$  of an ER fluid damper to the displacement  $x$ , the velocity  $\dot{x}$  and the electric field strength  $E$ :

$$F(x, \dot{x}, E) \approx \hat{F}(x, \dot{x}, E) = \sum_{i,j,k=0}^m C_{ijk} T_i(x') T_j(\dot{x}') T_k(E') \quad (30)$$

where the  $C_{ijk} \in \mathbb{R}$  denote the Chebyshev coefficients, and  $x'$ ,  $\dot{x}'$  and  $E'$  are normalised values. Conversely for the purpose of controlling an ER fluid device the electric field strength may also be approximated by a function  $\hat{E}(x, \dot{x}, |F|)$  of the displacement, the velocity and the (desired) damping force.

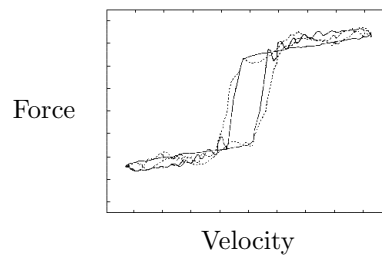


Figure 19: Comparison between the predicted ( ..... ) and the experimentally obtained ( — ) force-velocity characteristic for a Chebyshev polynomial fit (EHRGOTT and MASRI [15]).

A comparison between a force-velocity characteristic approximated by Chebyshev polynomials and the result of experiments conducted by EHRGOTT and MASRI [15] is provided in Figure 19. The predicted ER response resembles the corresponding experimental data. However, the force plots published by EHRGOTT and MASRI partly exhibit oscillatory behaviour which is frequently observed for polynomial interpolation. In addition, KAMATH and WERELEY [28] pointed out the computational effort to determine the large number of Chebyshev coefficients.

### 3.2.2 Neural networks

BURTON et al. [11] analysed the performance of a multilayer neural network to predict the electrorheological response. Neural networks consist of several processing units (neurons) whose inputs are weighted and passed to an activation (signal) function producing one single output. The weighting depends on the strength of the neurons' interconnections and can be adjusted by a kind of learning process (BURTON et al. [11]). The network presented by BURTON et al. was constructed by an algorithm known as the Dependence Identification Algorithm which is attributed to MOODY and ANTSAKLIS<sup>1</sup>. It was trained with different earthquake displacement histories and the corresponding responses of the considered seismic ER damper at varying field strengths.

MAKRIS et al. [38] extended the use of neural networks to a combination with mechanical models mentioned earlier. As the latter were assumed to reproduce most of the linear ER response, the above network was trained with the difference signal between the response predicted by the parametric models and the actual response of the damper.

<sup>1</sup>MOODY, S. O.; ANTSAKLIS, P. J.: The dependence identification neural network construction algorithm. IEEE Transactions on Neural Networks, New York, NY, 1995.

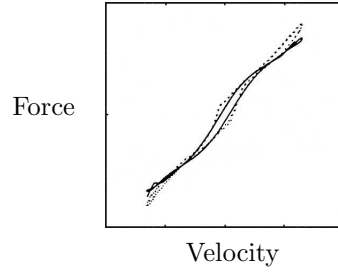


Figure 20: Comparison between the predicted ( — ) and the experimentally obtained ( ..... ) force-velocity characteristic for a neural network combined with the Maxwell model (MAKRIS et al. [38]).

BURTON et al. [11] found that the performance of the mere neural network was surpassed by discrete element models such as the Bingham model. When combined with simple mechanical models the network's prediction was partly superior to the results achieved with parametric methods alone. However, a conjunction with the more sophisticated BingMax model showed no improvements in simulating the ER fluid device (MAKRIS et al. [38]). A comparison between experimental data and a prediction obtained from the neural network combined with the parametric Maxwell model is shown in Figure 20.

## 4 Numerical simulation of a passive MR fluid vibration damper

In this section, simulation results are presented for a vehicle suspension design containing a magnetorheological vibration damper at a constant field strength, i. e., a passive magnetorheological fluid (MRF) damper; the latter was represented by mechanical models described above. The simulations conducted for a quarter vehicle model (cf. Figure 21) subject to different road excitations have been performed with MATLAB/SIMULINK 2.0<sup>2</sup>.

### 4.1 Quarter vehicle model

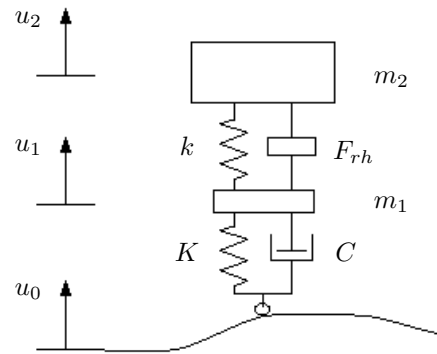


Figure 21: Quarter vehicle model with a passive MR fluid damper.

The equations of motion for the above depicted quarter vehicle model can be derived as

$$m_1 \ddot{u}_1 = K \cdot (u_0 - u_1) + C \cdot (\dot{u}_0 - \dot{u}_1) + k \cdot (u_2 - u_1) + F_{rh} \quad (31)$$

$$m_2 \ddot{u}_2 = -k \cdot (u_2 - u_1) - F_{rh}, \quad (32)$$

where  $m_1$  and  $m_2$  are the masses of the axle and the vehicle body,  $u_1$  and  $u_2$  denote their vertical displacement, and  $u_0$  is the road disturbance. Furthermore,  $K$  and  $C$  represent the spring and damping constants of wheel and tyre,  $k$  denotes the stiffness of the suspension, and  $F_{rh}$  is the force exerted by the MRF damper.

The mass parameters  $m_1 = 250$  kg and  $m_2 = 1300$  kg used for the following simulations correspond to the values of a small bus or utility vehicle; the stiffness  $K = 650000$  N/m and the damping rate  $C = 800$  Ns/m of the tyre, as well as the spring constant  $k = 110000$  N/m of the suspension have been adapted as for a typical ground vehicle (cf. HAĆ [21], MARGOLIS and GOSHTASBPUR [39]).

<sup>2</sup>N. N.: Using SIMULINK. The MathWorks, Natick, MA, 1997.

The MRF damper is reproduced by the Bingham model and the modified Bouc-Wen model described in the Sections 3.1.1 and 3.1.6. The performance of the quarter vehicle model subject to two different road disturbances is investigated (cf. KOSLIK et al. [32]).

A simple, conventional damper model is used for comparison. Its exerted force is given by

$$F = c \cdot (\dot{u}_2 - \dot{u}_1) \quad (33)$$

where the damping constant was chosen as  $c = 6000$  Ns/m.

#### 4.2 Bingham model of a passive MRF damper

In case of the Bingham model, the force generated by the MRF damper results from Equation (2) as

$$F_{rh} = f_c \cdot \text{sgn}(\dot{u}_2 - \dot{u}_1) + c_0(\dot{u}_2 - \dot{u}_1). \quad (34)$$

The parameter values used in the simulations correspond to the experimental data presented by SPENCER et al. [44] for the prototype of a magnetorheological fluid damper. Thus, the parameters related to the fluid's viscosity and the yield stress have been chosen as  $c_0 = 5000$  Ns/m and  $f_c = 670$  N.

#### 4.3 Bouc-Wen model of a passive MRF damper

The equations governing the force of the MRF damper in case of the modified Bouc-Wen model can be derived from the Equations (10), (11) and (12) yielding

$$F_{rh} = c_1(\dot{y} - \dot{u}_1) + k_1[(u_2 - u_1) - x_0] \quad (35)$$

where

$$\dot{y} = \frac{1}{c_0 + c_1} [\alpha z + c_0 \dot{u}_2 + c_1 \dot{u}_1 + k_0(u_2 - y)] \quad (36)$$

and

$$\dot{z} = -\gamma |\dot{u}_2 - \dot{y}| z |z|^{n-1} - \beta(\dot{u}_2 - \dot{y}) |z|^n + \delta(\dot{u}_2 - \dot{y}). \quad (37)$$

Likewise the parameters in this model have been chosen according to the data presented by SPENCER et al. [44] thus,  $c_0 = 5300$  Ns/m,  $c_1 = 93000$  Ns/m,  $k_0 = 1400$  N/m,  $k_1 = 540$  N/m,  $\alpha = 96300$  N/m,  $\beta = 2000000$  m<sup>-2</sup>,  $\gamma = 2000000$  m<sup>-2</sup>,  $n = 2$ ,  $\delta = 207$  and  $x_0 = 0$ .

#### 4.4 Simulation results for a step disturbance

Numerical results for the first disturbance resulting from a step with a height of 0.1 m at time  $t = 0$  (cf. KOSLIK et al. [32]) are depicted in Figs. 22–24.

For the passive MRF damper a faster decay of the excitation, especially in  $u_2$  is achieved as compared to the conventional device (Fig. 22). No significant difference is observed between the behavior of the Bingham and the modified Bouc-Wen model.

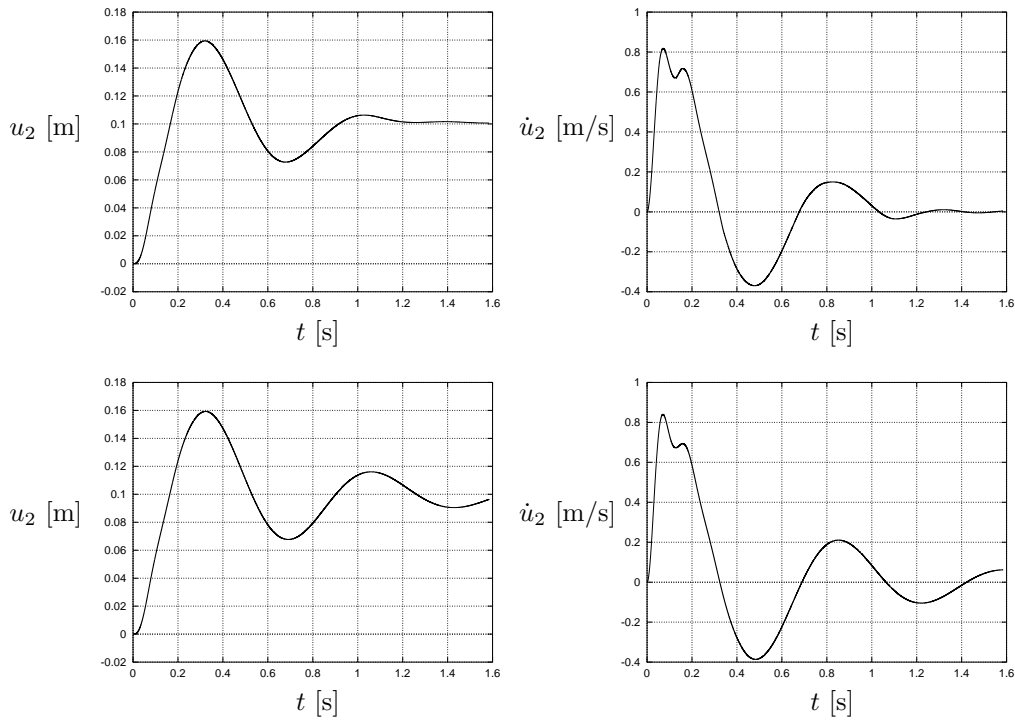


Figure 22: Simulation results for the quarter vehicle model subject to a step of height 0.1 m at initial time. Here, the results for the Bingham model and the modified Bouc-Wen model reproducing the performance of the MRF damper are quite similar (first row). A conventional viscous damper is used for comparison (second row). Left column: Vertical displacement of the vehicle body. Right column: Vertical velocity of the vehicle body.

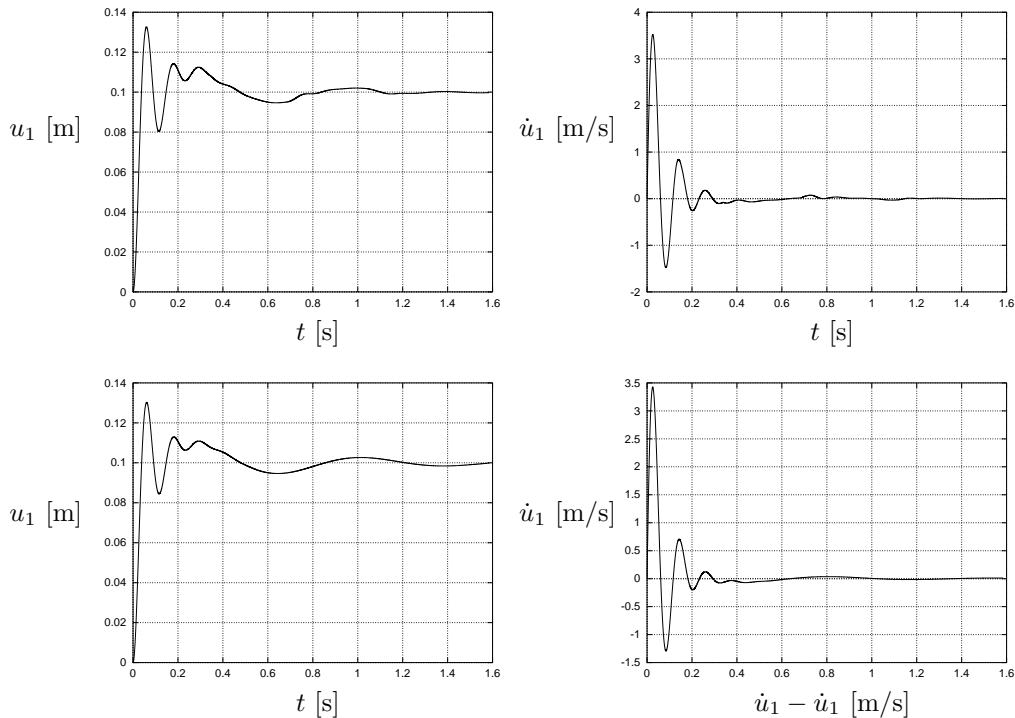


Figure 23: Simulation results for the quarter vehicle model subject to a step of height 0.1 m at initial time. The passive MRF damper is represented by the modified Bouc-Wen model (first row). The similar behavior of the Bingham model is omitted. A conventional viscous damper is used for comparison (second row). Left column: Vertical displacement of the vehicle axle. Right column: Vertical velocity of the vehicle axle.

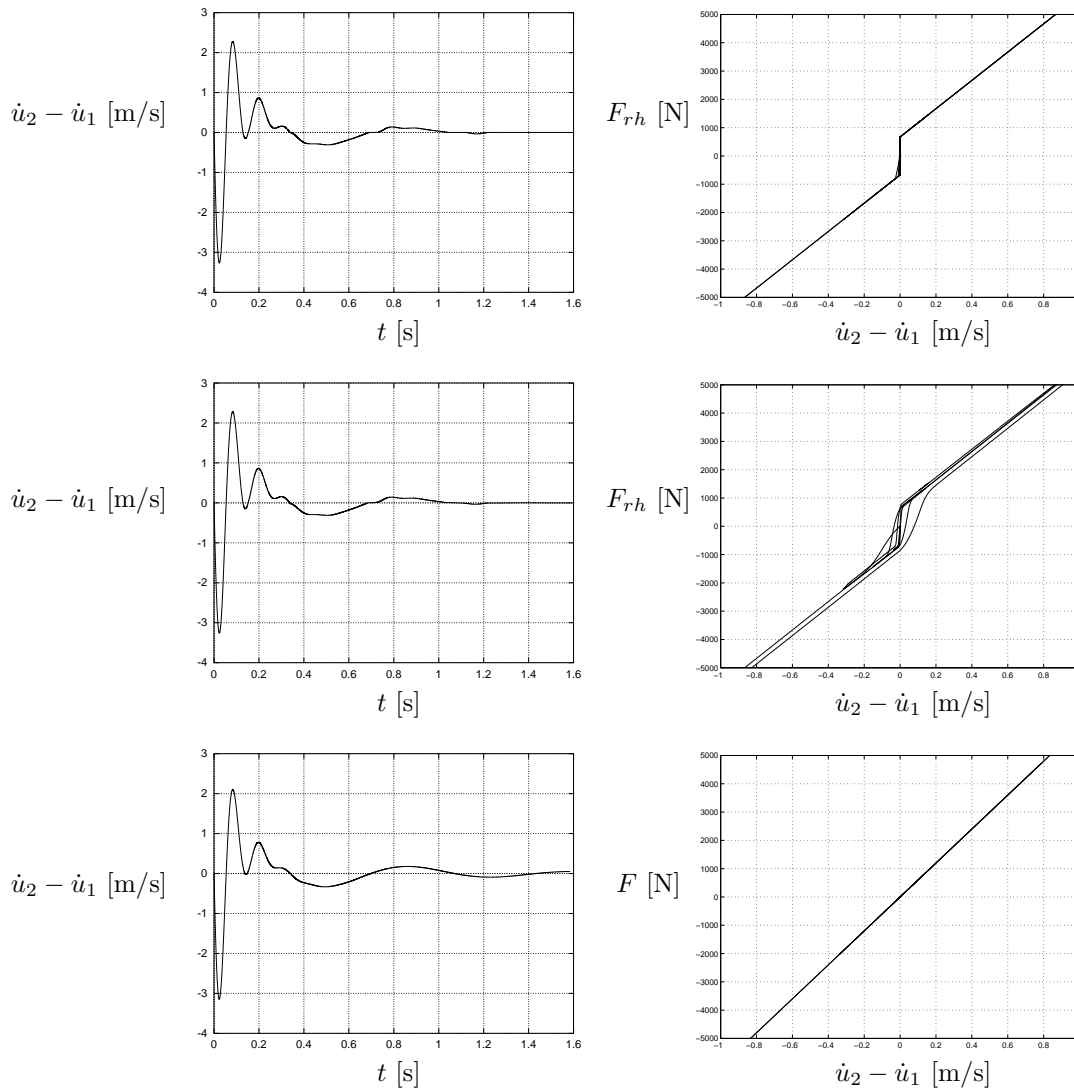


Figure 24: Simulation results for the quarter vehicle model subject to a step of height 0.1 m at initial time. The passive MRF damper is represented by the Bingham model (first row) and the modified Bouc-Wen model (second row). A conventional viscous damper is used for comparison (third row). Left column: Relative velocity between the vehicle body and the axle. Right column: Zoom into the force-velocity characteristic.

#### 4.5 Simulation results for a sinusoidal bump

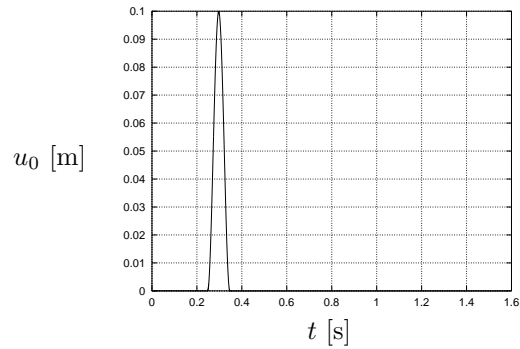


Figure 25: Disturbance signal simulating the ride over a sinusoidal bump with a maximum height of 0.1 m.

The second disturbance consists of a sinusoidal bump of the same maximum height of 0.1 m as depicted in Figure 25. The corresponding numerical results are displayed in Figs. 26–28.

The damping of the vibration is again faster for the passive MRF damper than for the conventional damper. For the sinusoidal bump, a slightly different behavior of the Bingham and the modified Bouc-Wen model can be observed, especially for the state  $u_2$  (Fig. 28).

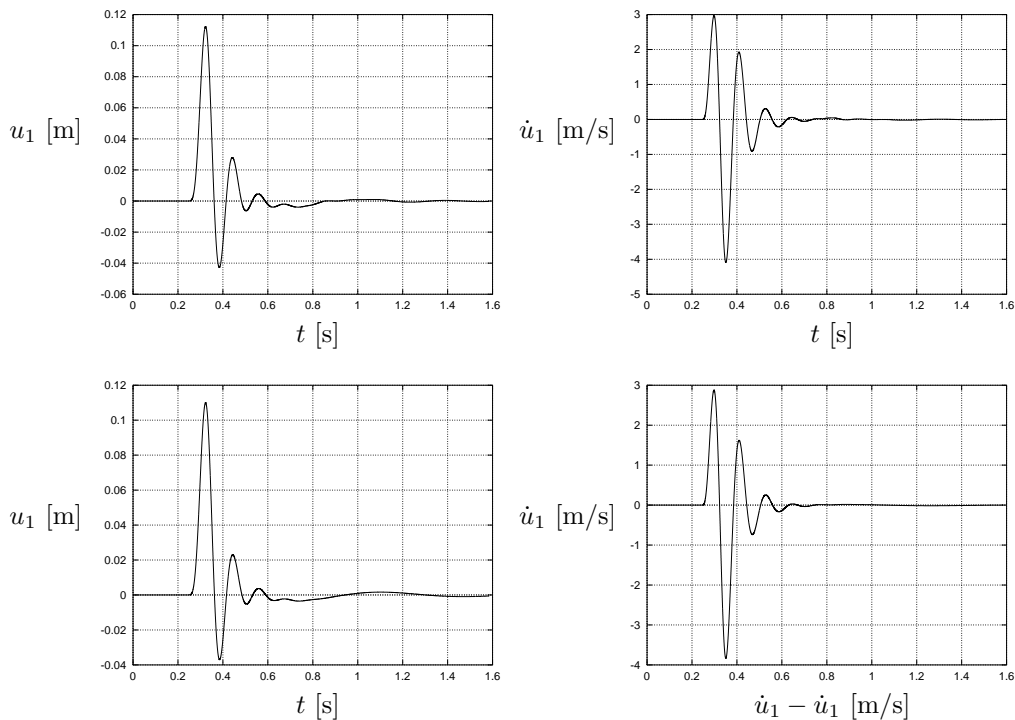


Figure 26: Simulation results for the quarter vehicle model subject to a sinusoidal bump of height 0.1 m. The passive MRF damper is represented by the modified Bouc-Wen model (first row). The similar performance of the Bingham model is omitted. A conventional viscous damper is used for comparison (second row). Left column: Vertical displacement of the vehicle axle. Right column: Vertical velocity of the vehicle axle.

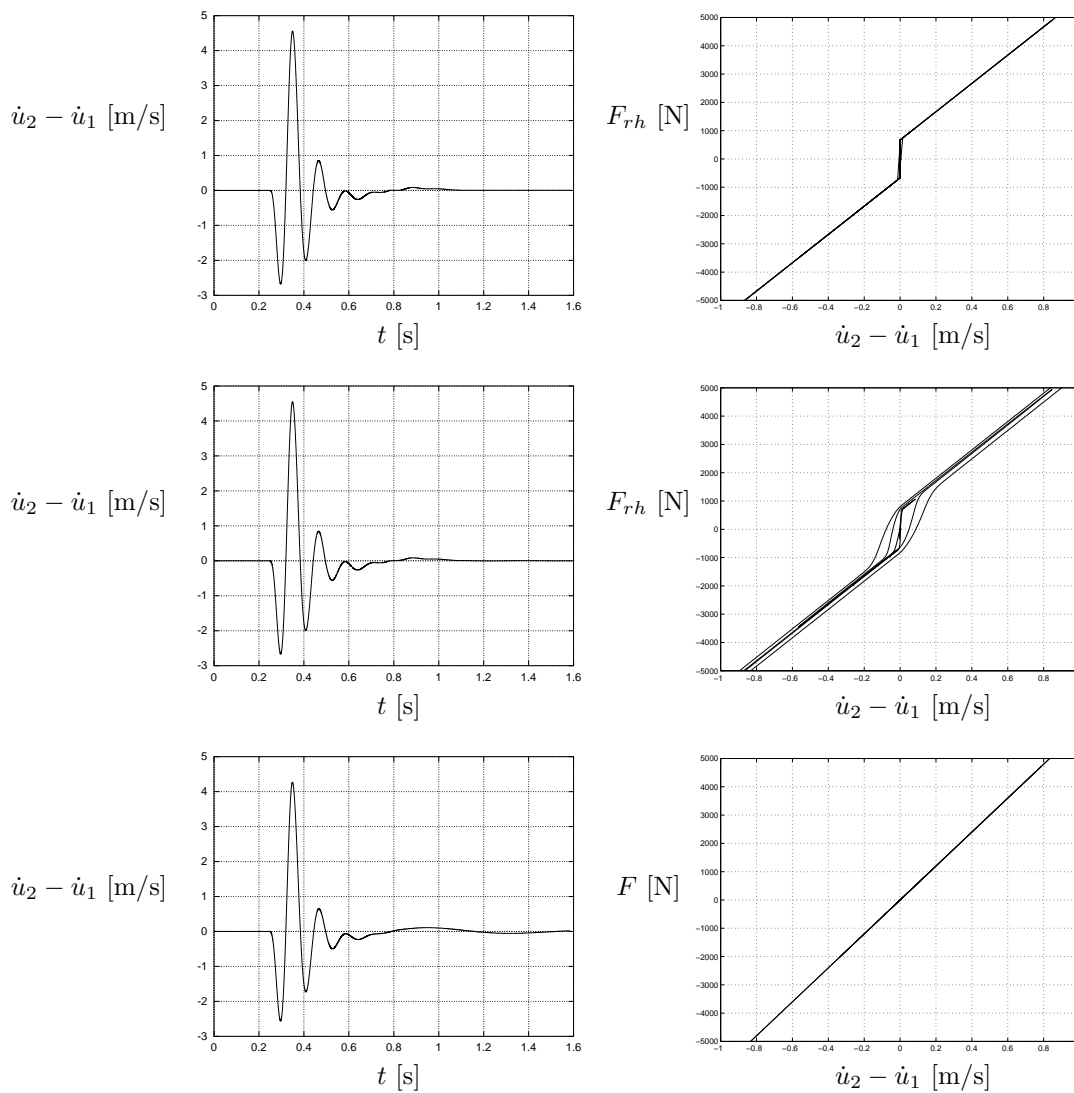


Figure 27: Simulation results for the quarter vehicle model subject to a sinusoidal bump of height 0.1 m. The passive MRF damper is represented by the Bingham model (first row) and the modified Bouc-Wen model (second row). A conventional viscous damper is used for comparison (third row). Left column: Relative velocity between vehicle body and axle. Right column: Zoom into the force-velocity characteristic.

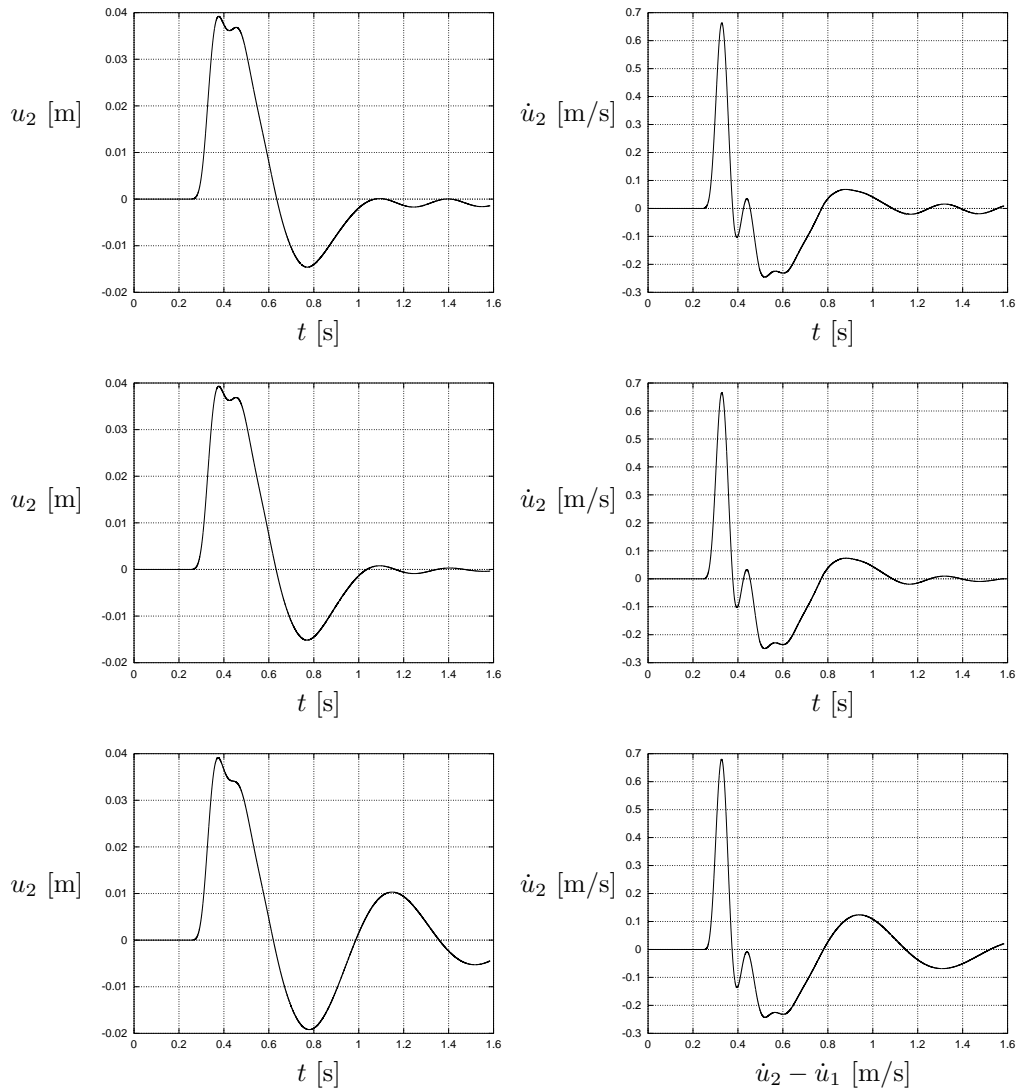


Figure 28: Simulation results for the quarter vehicle model subject to a sinusoidal bump of height 0.1 m. The passive MRF damper is represented by the Bingham model (first row) and the modified Bouc-Wen model (second row). A conventional viscous damper is used for comparison (third row). Left column: Vertical displacement of the vehicle body. Right column: Vertical velocity of the vehicle body.

## 5 Further applications of electro- and magnetorheological fluid devices

Adaptively controllable ER fluid devices to be used as shock absorbers in vehicles are described by HARTSOCK et al. [22] and PETEK [41]. Other automotive and related applications such as ER or MR clutches or engine mounts are investigated by HARTSOCK et al. [22], LAMPE et al. [34] and WHITTLE et al. [50]. BACKÉ et al. [3] developed an ER fluid servo drive in a joint project with Bayer AG and Carl Schenck AG. Adaptively controllable MR fluid devices are now available for semi-active vibration damping of driver seats in trucks and as rotational brakes for controllable resistance in aerobic exercise equipment (LORD CORPORATION [36], JOLLY et al. [24]). An ER fluid damper for semi-active control of vibrations of a flexible, lightweight robot arm is described by LI et al. [35]. MR fluid devices for seismic protection of structures are investigated by CARLSON and SPENCER [12], DYKE et al. [14] and the LORD CORPORATION [36]. ER fluid devices for this purpose are described by BURTON et al. [11]. CHOI et al. [13] investigate the vibration characteristics of a composite beam filled with an electrorheological fluid. The application of electroviscous fluids as movement sensor control devices in active vibration dampers is discussed by OPPERMANN et al. [40]. MR fluid lag mode dampers for helicopters with hingeless and bearingless rotors which improve aeromechanical stability with respect to air and ground resonance are mentioned by KAMATH et al. [30].

Many more designs and applications of electro- and magnetorheological fluid devices can be expected in the near future.

## 6 Conclusions and outlook

The basic properties of electro- and magnetorheological fluids as well as various models for electro- and magnetorheological fluid devices, especially vibration dampers, and their applications have been discussed in this paper. However, there is still a need for rigorous mathematical models which accurately describe electro- and magnetorheological fluids and devices, and which are suitable for understanding, investigating and predicting their behaviour by numerical simulation.

Furthermore, to fully utilize the innovative potential of adaptively controllable electro- and magnetorheological fluid devices, (optimal) control strategies must be developed taking into account the dynamical behaviour of the specific complex mechanical system including the controllable ER or MR fluid device. For example, when using a semi-active suspension based on controllable ER fluid shock absorbers, the full dynamical behavior of the vehicle, the ER fluid dampers and the road disturbances must be considered in order to maximize the driving comfort and the safety of a car by adaptive damping and level control [23]. For this purpose, models for actively controllable ER and MR fluid devices must be developed describing the dynamical behaviour of a specific device with respect to changes in the electric or magnetic field.

**Acknowledgement.** The authors gratefully acknowledge the support by the German science foundation *Deutsche Forschungsgemeinschaft (DFG)* within the project C4 of the collaborative research center *Sonderforschungsbereich 438*. The authors also gratefully acknowledge the support given by Prof. Dr. Dr.h.c. R. Bulirsch (Technische Universität München). The authors are indebted for helpful and stimulating discussions to Prof. Dr. B.F. Spencer, Jr. (University of Notre Dame, Illinois), Dr. H. Rosenfeldt and Dipl.-Ing. L. Johnston (Schenck Pegasus GmbH, Darmstadt), Dr. H. Böse (Fraunhofer Institut für Silicatforschung, Würzburg), Prof. Dr. R.H.W. Hoppe (Universität Augsburg), and Dipl.-Math. U. Rettig (Technische Universität München).

## References

- 1 ANONYMOUS: Provisional product information Rheobay TP AI 3565 and Rheobay TP AI 3566. Bayer AG, Leverkusen, 1994.
- 2 ANONYMOUS: RheAct — Der hochdynamische rheo-elektrische Actuator. Carl Schenck AG, Darmstadt, 1998.
- 3 BACKÉ, W.; FEES, G.; MURRENHOF, H.: Innovative Fluidtechnik — Hochdynamischer Servoantrieb mit elektrorheologischen Flüssigkeiten. *Ölhydraulik und Pneumatik (o+p)*, **41** (1997) 11/12.
- 4 BIRD, B.; ARMSTRONG, R.; HASSAGER, O.: Dynamics of polymeric liquids. J. Wiley and Sons, New York, 1987.
- 5 BLOCK, H.; KELLY, J. P.: Electro-rheology. *Journal of Physics D: Applied Physics*, **21** (1988), 1661-1677.
- 6 BONNECAZE, R. T.; BRADY, J. F.: Dynamic simulation of an electrorheological fluid. *Journal of Chemical Physics*, **96** (1992), 2183-2202.
- 7 BONNECAZE, R. T.; BRADY, J. F.: Yield stresses in electrorheological fluids. *Journal of Rheology*, **36** (1992), 73-115.
- 8 BÖSE, H.: Private communication. October 1998.
- 9 BROKATE, M.; SPREKELS, J.: Hysteresis and Phase Transitions. Springer-Verlag, New York, 1996.

- 10 BURTON, S. A.: Design and analysis of an electrorheological damper for seismic protection of structures. MS Thesis, University of Notre Dame, IN, 1996.
- 11 BURTON, S. A.; MAKRIS, N.; KONSTANTOPOULOS, I.; ANTSAKLIS, P. J.: Modeling the response of ER damper: phenomenology and emulation. *Journal of Engineering Mechanics*, **122** (1996), 897-906.
- 12 CARLSON, J. D.; SPENCER JR., B. F.: Magneto-rheological fluid dampers: scalability and design issues for application to dynamic hazard mitigation. In *Proceedings of the 2nd International Workshop on Structural Control*, Hong Kong, 18-21 December 1996, 99-109.
- 13 CHOI, Y.; SPRECHER, A. F.; CONRAD, H.: Vibration characteristics of a composite beam containing an electrorheological fluid. *Journal of Intelligent Material Systems and Structures*, **1** (1990), 91-104.
- 14 DYKE, S. J.; SPENCER JR., B. F.; SAIN, M. K.; CARLSON, J. D.: On the efficacy of magnetorheological dampers for seismic response reduction. 1997 ASME Design Engineering Technical Conferences, Sacramento, CA, 14-17 September 1997.
- 15 EHRGOTT, R. C.; MASRI, S. F.: Modeling the oscillatory dynamic behavior of electrorheological materials in shear. *Smart Materials and Structures*, **1** (1992), 275-285.
- 16 ENGELMANN, B.; HIPTMAIR, R.; HOPPE, R. H. W.; MAZURKEVITCH, G.: Numerical simulation of electrorheological fluids based on an extended Bingham model. Preprint SFB-438-9902, Sonderforschungsbereich 438, Technische Universität München – Universität Augsburg, 1999. World Wide Web: <http://www-lit.mathematik.tu-muenchen.de/veroeff/html/SFB/992.76001.html>.
- 17 GAMOTA, D. R.; FILISKO, F. E.: Dynamic mechanical studies of electrorheological materials: Moderate frequencies. *Journal of Rheology*, **35** (1991), 399-425.
- 18 GAST, A. P.; ZUKOSKI, C. F.: Electrorheological fluids as colloidal suspensions. *Advances in Colloid and Interface Science*, **30** (1989), 153-202.
- 19 GAVIN, H. P.; HANSON, R. D.; FILISKO, F. E.: Electrorheological dampers, Part I: Analysis and design. *Journal of Applied Mechanics*, **63** (1996), 669-675.
- 20 GAVIN, H. P.; HANSON, R. D.; FILISKO, F. E.: Electrorheological dampers, Part I: Testing and modeling. *Journal of Applied Mechanics*, **63** (1996), 676-682.
- 21 HAĆ, A.: Optimal linear preview control of active vehicle suspension. *Vehicle System Dynamics*, **21** (1992), 167-195.
- 22 HARTSOCK, D. L.; NOWAK, R. F.; CHAUNDY, G. J.: ER fluid requirements for automotive devices. *Journal of Rheology*, **35** (1991), 1305-1326.
- 23 HOPPE, R. H. W.; MAZURKEVITCH, G.; RETTIG, U.; VON STRYK, O.: Modeling, simulation and control of electrorheological fluid devices. In BUNGARTZ, H.-J. et al., editors: *Lectures on Applied Mathematics*, pages 251-276. Springer-Verlag, Berlin, 2000.
- 24 JOLLY, M. R.; BENDER, J. W.; CARLSON, J. D.: Properties and applications of commercial magnetorheological fluids. SPIE 5th Annual Int. Symposium on Smart Structures and Materials, San Diego, CA, 15 March 1998.
- 25 JOLLY, M. R.; CARLSON, J. D.; MUÑOZ, B. C.: A model of the behaviour of magnetorheological materials. *Smart Materials and Structures*, **5** (1996), 607-614.
- 26 KAMATH, G. M.; HURT, M. K.; WERELEY, N. M.: Analysis and testing of Bingham plastic behavior in semi-active electrorheological fluid dampers. *Smart Materials and Structures*, **5** (1996), 576-590.
- 27 KAMATH, G. M.; WERELEY, N. M.: System identification of ER fluid dampers using a nonlinear mechanisms-based model. 1996 SPIE Conference on Smart Materials and Structures, Paper No. SPIE-2717-46, San Diego, CA, 25-29 February 1996.
- 28 KAMATH, G. M.; WERELEY, N. M.: A nonlinear viscoelastic-plastic model for electrorheological fluids. *Smart Materials and Structures*, **6** (1997), 351-359.
- 29 KAMATH, G. M.; WERELEY, N. M.: System identification of electrorheological fluid-based dampers using a nonlinear viscoelastic-plastic phenomenological model. 35th Aerospace Sciences Meeting, Paper No. AIAA-97-0359, Reno, NV, 6-9 January 1997.
- 30 KAMATH, G. M.; WERELEY, N. M.; JOLLY, M. R.: Analysis and testing of a model-scale magnetorheological fluid helicopter lag mode damper. American Helicopter Society 53rd Annual Forum, Virginia Beach, 29 April - 1 May 1997, 1325-1335.
- 31 KLINGENBERG, D. J.; VAN SWOL, F.; ZUKOSKI, C. F.: Dynamic simulation of electrorheological suspensions. *Journal of Chemical Physics*, **91** (1989), 7888-7895.
- 32 KOSLIK, B.; RILL, G.; VON STRYK, O.; ZAMPIERI, D. E.: Active suspension design for a tractor by optimal control methods. Preprint SFB-438-9801, Sonderforschungsbereich 438, Technische Universität München – Universität Augsburg, 1999. World Wide Web: <http://www-lit.mathematik.tu-muenchen.de/veroeff/html/SFB/982.49003.html>.
- 33 LAMPE, D., Materials database on commercially available electro- and magnetorheological fluids. Institut für Luft- und Raumfahrttechnik, Technische Universität Dresden, 1997. World Wide Web: <http://www.tu-dresden.de/mw/ilr/lampe/HAUENG.HTM>.
- 34 LAMPE, D.; THESS, A.; DOTZAUER, C.: MRF clutch — Design considerations and performance. In *Proceedings of the Actuator 98*, Bremen, 17-19 June 1998.
- 35 LI, J.; JIN, D.; ZHANG, X.; ZHANG, J.; GRUVER, W. A.: An electrorheological fluid damper for robots. In *Proceedings of the 1995 IEEE International Conference on Robotics and Automation*, Vol. 3, Nagoya, Japan, 21-27 May 1995, 2631-2636.
- 36 LORD CORPORATION: Rheonetic MagnetoRheological (MR) Fluid Technology. Cary, NC, 1997. World Wide Web: <http://www.mrfluid.com/>.

- 37 MAKRIS, N.; BURTON, S. A.; HILL, D.; JORDAN, M.: Analysis and design of ER damper for seismic protection of structures. *Journal of Engineering Mechanics*, **122** (1996), 1003-1011.
- 38 MAKRIS, N.; BURTON, S. A.; TAYLOR, D. P.: Electrorheological damper with annular ducts for seismic protection applications. *Smart Materials and Structures*, **5** (1996), 551-564.
- 39 MARGOLIS, D. L.; GOSHTASBPOUR, M.: The chatter of semi-active on-off suspensions and its cure. *Vehicle System Dynamics*, **13** (1984), 129-144.
- 40 OPPERMAN, G.; PENNERS, G.; SCHULZE, M.; MARQUARDT, G.; FLINDT, R.; NAUMANN, T. H.: Applications of electroviscous fluids as movement sensor control devices in active vibration dampers. In CARLSON, J. D., editor: *Proceedings of the International Conference on Electrorheological Fluids*, Raleigh, NC, February 1989, 287-299.
- 41 PETEK, N. K.: An electronically controlled shock absorber using electrorheological fluid. Society of Automotive Engineers Technical Paper Series, Paper No. 920275, 1992.
- 42 POWELL, J. A.: Modelling the oscillatory response of an electrorheological fluid. *Smart Materials and Structures*, **3** (1994), 416-438.
- 43 SPENCER JR., B. F.: Recent trends in vibration control in the U.S.A. In *Proceedings of the 3rd International Conference on Motion and Vibration Control, Vol. 2*, Chiba, Japan, 1-6 September 1996, K1-K6.
- 44 SPENCER JR., B. F.; DYKE, S. J.; SAIN, M. K.; CARLSON, J. D.: Phenomenological model of a magnetorheological damper. *Journal of Engineering Mechanics*, **123** (1997), 230-238.
- 45 STANWAY, R.; SPROSTON, J. L.; STEVENS, N. G.: Nonlinear modelling of an electro-rheological vibration damper. *Journal of Electrostatics*, **20** (1987), 167-184.
- 46 STANWAY, R.; SPROSTON, J. L.; EL-WAHED, A. K.: Applications of electro-rheological fluids in vibration control: a survey. *Smart Materials and Structures*, **5** (1996), 464-482.
- 47 STOER, J.; BULIRSCH, R.: *Introduction to Numerical Analysis*. 2nd edition, Springer, Berlin, 1993.
- 48 WEISS, W. D.; DUCLOS, T. G.; CARLSON, J. D.; CHRZAN, M. J.; MARGIDA, A. J.: High strength magneto- and electro-rheological fluids. Society of Automotive Engineers Technical Paper Series, Paper No. 932451, 1993.
- 49 WEN, Y.: Method for random vibration of hysteretic systems. *Journal of the Engineering Mechanics Division*, **102** (1976), 249-263.
- 50 WHITTLE, M.; ATKIN, R. J.; BULLOUGH, W. A.: Fluid dynamic limitations on the performance of an electrorheological clutch. *Journal of Non-Newtonian Fluid Mechanics*, **57** (1995), 61-81.
- 51 WINSLOW, W. M.: Induced vibration of suspensions. *Journal of Applied Physics*, **20** (1949), 1137-1140.

Received January 7, 1997, revised June 1, 1997, final revision March 13, 1997, accepted April 15, 1998

*Address:* TORSTEN BUTZ; Dr. OSKAR VON STRYK, Lehrstuhl M2 Höhere Mathematik und Numerische Mathematik, Technische Universität München, D-80290 München, Germany, email: [butz,stryk@ma.tum.de](mailto:butz,stryk@ma.tum.de)